The Astrophysical Journal, 694:867–878, 2009 April 1 doi:10.1088/0004-637X/694/2/867

THE EVOLUTION OF THE $M_{\rm BH}$–σ RELATION INFERRED FROM THE AGE DISTRIBUTION OF LOCAL EARLY-TYPE GALAXIES AND ACTIVE GALACTIC NUCLEI EVOLUTION

Francesco Shankar[1], Mariangela Bernardi[2], and Zoltán Haiman[3]
[1] Department of Astronomy, The Ohio State University, Columbus, OH 43210, USA; shankar@astronomy.ohio-state.edu
[2] Department of Physics and Astronomy, University of Pennsylvania, 209 South 33rd St., Philadelphia, PA 19104, USA; bernardm@physics.upenn.edu
[3] Department of Astronomy, Columbia University, 550 West 120th Street, New York, NY 10027, USA; zoltan@astro.columbia.edu
Received 2008 April 18; accepted 2008 June 19; published 2009 March 20

ABSTRACT

We utilize the local velocity dispersion function (VDF) of spheroids, together with their inferred age distributions, to predict the VDF at higher redshifts ($0 < z \lesssim 6$), under the assumption that (1) most of the stars in each nearby spheroid formed in a single episode and, (2) the velocity dispersion σ remained nearly constant afterward. We assume further that a supermassive BH forms concurrently with the stars, and within ± 1 Gyr of the formation of the potential well of the spheroid, and that the relation between the mass of the BH and host velocity dispersion maintains the form $M_{\rm BH} \propto \sigma^{\beta}$ with $\beta \approx 4$, but with the normalization allowed to evolve with redshift as $\propto (1+z)^{\alpha}$. We compute the BH mass function associated with the VDF at each redshift, and compare the accumulated total BH mass density with that inferred from the integrated quasar luminosity function (LF; the so-called Sołtan argument). This comparison is insensitive to the assumed duty cycle or Eddington ratio of quasar activity, and we find that the match between the two BH mass densities favors a relatively mild redshift evolution, with $\alpha \sim 0.33$, with a positive evolution as strong as $\alpha \gtrsim 1.3$ excluded at more than 99% confidence level. A direct match between the characteristic BH mass in the VDF-based and quasar LF-based BH mass functions also yields a mean Eddington ratio of $\lambda \sim 0.5$–1 that is roughly constant within $0 \lesssim z \lesssim 3$. A strong positive evolution in the $M_{\rm BH}$–σ relation is still allowed by the data if galaxies increase, on average, their velocity dispersions since the moment of formation due to dissipative processes. If we assume that the mean velocity dispersion of the host galaxies evolves as $\sigma(z) = \sigma(0) \times (1+z)^{-\gamma}$, we find a lower limit of $\gamma \gtrsim 0.23$ for $\alpha \gtrsim 1.5$. The latter estimate represents an interesting constraint for galaxy evolution models and can be tested through hydro simulations. This dissipative model, however, also implies a decreasing λ at higher z, at variance with several independent studies.

Key words: black hole physics – galaxies: active – galaxies: evolution

1. INTRODUCTION

It has now been assessed that most, if not all, local galaxies have a supermassive black hole (BH) at their center, the mass of which is tightly correlated with the velocity dispersion σ and other bulk properties of the host galaxy (e.g., Ferrarese & Merritt 2000; Gebhardt et al. 2000). However, the sample of local galaxies for which the BH sphere of influence has been resolved amounts to only ∼30. It is not clear how representative this small sample is of the whole BH population, and whether the correlations seen in the sample already held in the past.

Peng et al. (2006) have collected a sample of 31 lensed and 18 nonlensed active galactic nuclei (AGNs) at redshifts $z > 1.7$. They measured rest-frame R-band luminosities from H-band fluxes and BH masses by applying virial relations based on emission line widths. They found that the BH-to-host galaxy luminosity at $z \sim 2$ is about the same as that at $z \sim 0$. Therefore, once the observed rest-frame luminosity is dimmed through passive evolution to $z \sim 0$, at fixed BH mass the ratio BH-to-host luminosity grows significantly, and the resulting BH-luminosity normalization is several times higher than the local one. Similar results were derived by McLure et al. (2006), who measured the BH-to-host galaxy mass ratio in a sample of radio-loud AGNs in the redshift range $0 < z < 2$ finding $M_{\rm BH}/M_{\rm STAR} \propto (1+z)^2$. Shields et al. (2006) found that the CO emission lines in a sample of $z > 3$ quasars are very narrow, suggesting bulge mass about an order of magnitude lower than measured in the local universe, at fixed BH mass (see also Coppin et al. 2008). Treu et al. (2007) found that the BH masses in a sample of 20 Seyferts galaxies at $z = 0.36$ are offset by an amount of $\Delta \log M_{\rm BH} \sim 0.5$ at fixed velocity dispersion, which implies an evolution of $M_{\rm BH}/M_{\rm STAR} \propto (1+z)^{1.5 \pm 1.0}$, consistent with that derived by the previous works.

On the other hand, Lauer et al. (2007) have discussed several possible biases which may seriously affect these findings. At high redshifts a sample will be biased toward the most luminous AGNs and more massive BHs. Given the observed scatter in the local relations, especially significant in the $M_{\rm BH}$–host luminosity relation, these massive BHs will be preferentially associated with the less massive, but more numerous galaxies, yielding a false sign of evolution. When the cumulative mass density of AGNs is taken into account, several authors (e.g., Haiman et al. 2004; Marconi et al. 2004; Silverman et al. 2008; Shankar et al. 2009, hereafter SWM) have shown that once rescaled by a simple constant, it provides a good match to the cosmological star formation rate density. De Zotti et al. (2006) and SWM have shown that the galaxy stellar mass function at $z \sim 2$, mostly composed of massive early-type galaxies (e.g., Drory et al. 2005), converted into a BH mass density assuming an $M_{\rm BH}/M_{\rm STAR}$ ratio three to five times higher than in the local universe, would imply a BH mass density already close, if not higher, than that inferred in the local universe, leaving no room for further accretion at $z \lesssim 2$, where, in fact, a significant fraction of the total AGN energy output is produced. Recently, Ho et al. (2007) compiled a sample of 154 nearby ($z < 0.1$) active galaxies showing substantial ongoing BH growth in the most actively accreting AGNs, where BH growth appears to be delayed with respect to the assembly of the host galaxy.

In this paper, we propose a simple, yet robust, way to constrain the degree of redshift evolution in the $M_{\rm BH}$–σ relation, that

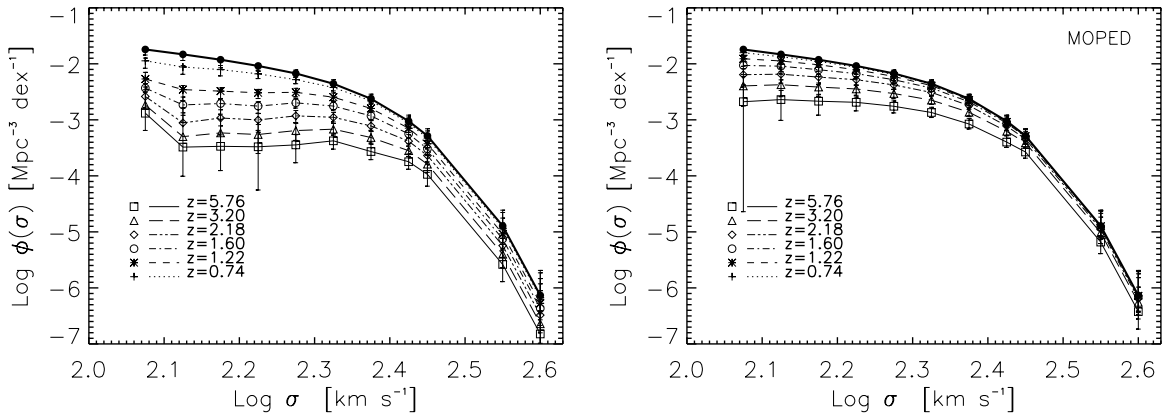

Figure 1. VDF at different redshifts, as labeled, obtained by combining the local VDF with the age distribution of local galaxies (Equation (1)). Left panel: VDF obtained using the ages computed from Lick indexes; right panel: VDF obtained using the ages computed from the MOPED algorithm (see the text for details).

is relatively insensitive to assumptions that relate the SMBH population to quasars. We combine the measured VDF of local spheroids with a postulated power-law redshift dependence of the $M_{\rm BH}$–σ relation. By comparing the resulting total BH mass density at each redshift with the same quantity inferred from integration of the AGN LF (see Sołtan 1982), we find the degree of evolution required in the $M_{\rm BH}$–σ relation to match these two independent estimates. This approach yields results based on the "bulk" of the active BHs at all redshifts, and is therefore relatively insensitive to possible biases which may affect studies performed on small samples of high-redshift luminous quasars (e.g., Lauer et al. 2007). After describing the sample used in our computations in Section 2, we proceed to derive our main results in Section 3. These results are discussed further in Section 5, where we also offer our conclusions. Throughout this paper we use the cosmological parameters $\Omega_m = 0.30$, $\Omega_\Lambda = 0.70$, and $h \equiv H_0/100\,{\rm km\,s^{-1}\,Mpc^{-1}} = 0.7$, consistent with the three- (Spergel et al. 2007) and five-year (Dunkley et al. 2009) data from the *Wilkinson Microwave Anisotropy Probe (WMAP)*.

2. DATA

We have used the sample of early-type galaxies obtained by Bernardi et al. (2006). The sample, extracted from the Sloan Digital Sky Survey (York et al. 2000), contains over 40,000 early-type galaxies, selected for having an apparent magnitude $14.5 \lesssim M_r \lesssim 17.75$, extending over a redshift range $0.013 < z < 0.25$, which corresponds to a maximum look-back time of 3 Gyr. The ages of galaxies are computed in two different ways, discussed in detail by Jimenez et al. (2007), from (1) single stellar population spectral fitting, using the MOPED algorithm (Heavens et al. 2000) to determine the full star-formation history of the galaxies and (2) using the published ages by Bernardi et al. (2006) which were obtained by fitting the Thomas et al. (2005) α-enhanced models to the Lick index absorption features measured from stacked spectra of galaxies with similar properties. The age distributions at fixed velocity dispersion σ are generally broad, but tend to be narrower and centered on older ages for higher values of σ. Such effects are more marked for the age distributions inferred from MOPED (see Figure 1 in Haiman et al. 2007). We will compare results obtained by adopting either the MOPED or the Lick-index age distribution in Section 3.

The analysis presented in Bernardi et al. (2006); Haiman et al. (2007) probe velocity dispersions within $2.05 \lesssim \log(\sigma/{\rm km\,s^{-1}}) \lesssim 2.45$. Here we extend such analysis including the age distributions of galaxies with velocity dispersion $2.45 \lesssim \log(\sigma/{\rm km\,s^{-1}}) \lesssim 2.55$. We find that galaxies within this last bin are even older than the oldest galaxies probed by Haiman et al. (2007), confirming and extending the general trend of increasing age for larger σ. Instead of considering one single bin with mean velocity dispersion $\log(\sigma/{\rm km\,s^{-1}}) = 2.5$, we have treated the bin as two distinct bins with $\log(\sigma/{\rm km\,s^{-1}}) = 2.45$ and 2.55 which we have assumed share the same age distributions as the total bin. We have also included an additional bin with $\log(\sigma/{\rm km\,s^{-1}}) = 2.60$, which we have again assumed to have an age distribution equal[4] to that with $\log(\sigma\,{\rm km\,s^{-1}}) = 2.45$ and 2.55 (a direct estimate of the ages for these galaxies with the techniques discussed above is highly limited by the low signal-to-noise of the spectra). As will be shown in Section 3 (Figure 1), this binning in $\log\sigma$ enables us to better probe the statistical evolution of the VDF even at large velocity dispersions, and it has a negligible effect in the resulting cumulative BH mass density and on our general results.

3. RESULTS

We first estimate the VDF as a function of redshift z. At any z, the VDF in a given bin of velocity dispersion σ_i is given by all the galaxies which have formed prior to z. Therefore, to compute $\Phi(\sigma_j, z)$ we subtract from the local census of galaxies with velocity dispersion σ_i those galaxies that have an age τ lower then the look-back time $\tau_j(z)$:

$$\Phi(\sigma_i, z) = \left[1 - \sum_{\tau<\tau_j} p(\tau_j(z)|\sigma_i)\right] \times \Phi(\sigma_i)\,. \qquad (1)$$

Note that $p(\tau_j(z)|\sigma_i)$ refers to the fraction of galaxies with velocity dispersion σ_i which have an age of $\tau_j(z) \pm 1$ Gyr. Therefore, $\Phi(\sigma_i, z)$ includes in the σ_i bin all galaxies whose ages are within ± 1 Gyr of $\tau_j(z)$. The VDF at $z = 0$ is taken from Sheth et al. (2003) and includes the contribution of bulges of spirals. We therefore assume that bulges of spirals and local spheroids within the same bin of velocity dispersion share similar age distributions. However, as discussed in Section 5, our results would still hold even if the contribution from spirals were neglected. The statistical uncertainties associated with $\Phi(\sigma, z)$

[4] A more appropriate choice would be to assign older ages to the galaxies with extreme velocity dispersions, given the general trend of older ages for higher σ, however, this would pose even stronger evidence for the downsizing discussed below further strengthening our general conclusions.

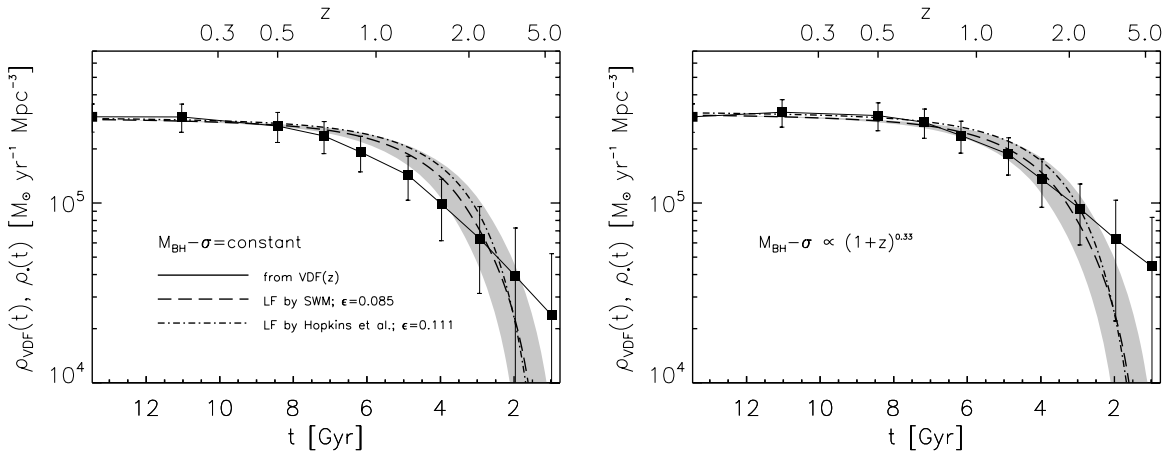

Figure 2. Comparison between the accreted mass density at each redshift obtained from $\Phi(\sigma, z)$, convolved with the local M_{BH}–σ relation (*solid* curve and solid squares) and the mass density inferred from integration of the Shankar et al. (2009) AGN LF (long-dashed curve) and a radiative efficiency of $\epsilon = 0.077$; the gray area represents the uncertainty at each time t associated with the mass accreted within $t \pm 1$ Gyr; the dot-dashed line is the predicted accreted mass using the Hopkins et al. (2007) AGN LF and a radiative efficiency of $\epsilon = 0.114$. The left panel shows $\rho_{VDF}(z)$ predicted from the VDF assuming that the M_{BH}–σ relation is independent of redshift, while the right panel shows the predictions for the best-fit $\rho_{VDF}(z)$ when the normalization of the M_{BH}–σ relation evolves as $\propto (1+z)^{0.33}$.

are computed from Equation (1) through error propagation including random uncertainties in $p(\tau_j(z)|\sigma)$, given by Haiman et al. (2007; see their Figure 1) and $\Phi(\sigma)$, given by Sheth et al. (2003).

Figure 1 shows the VDF obtained from Equation (1). The different curves in both panels show $\Phi(\sigma, z)$ at different redshifts, as labeled. At fixed redshift, the symbols indicate the position of the mean in the bin of $\log\sigma$ considered, for which the reliable age distributions $p(\tau_j(z)|\sigma_i)$ have been computed. In the left panel of Figure 1, the p_{ji} distributions have been derived from the Lick-indices method, while the right panel shows the results with the MOPED-based p_{ji} distributions. In our analysis below, we will adopt the $\Phi(\sigma, z)$ implied by the p_{ji} derived from Lick indices. However, we will discuss the consequences of the alternate choice on our results in Section 4. In both cases, we reproduce the conclusion of previous work (e.g., Trager et al. 2000; Thomas et al. 2005; Bernardi et al. 2006; Jimenez et al. 2007; Haiman et al. 2007)—that is, we find strong evidence for *downsizing*: on average, galaxies with larger velocity dispersion are formed earlier. This behavior is expected from basic galaxy formation theory: high-redshift galaxies form in a denser universe and therefore preferentially form out of baryonic clumps collapsed in denser, gas-rich environments which in turn, induce more dissipation, more compact remnants, and higher velocity dispersions. At fixed velocity dispersion, the MOPED ages are higher than inferred from Lick indices, producing a less pronounced evolution in the VDF at $0 \lesssim z \lesssim 3$. Theoretical models in which the galaxy velocity dispersion is linked with the virial velocity of the host halo (e.g., Ferrarese 2002) predict similar trends for the VDF as a function of time (Cirasuolo et al. 2005; see also Loeb & Peebles 2003).

The BH mass function implied by the VDF at any time is given by converting $\Phi(\sigma, z)$ to a BH mass function through the M_{BH}–σ relation and a convolution with a Gaussian with intrinsic scatter of 0.22 dex. We assume here that $\log M_{BH}$ at fixed $\log\sigma$ is given by a Gaussian distribution, with a mean of

$$\log\left(\frac{M_{BH}}{M_\odot}\right) = 8.21 + 3.83\log\left(\frac{\sigma}{200\ \mathrm{km\ s^{-1}}}\right) + \alpha\log(1+z)\,, \quad (2)$$

and a standard deviation of $\eta = 0.22$. This latter value represents the intrinsic scatter as given by Tundo et al. (2007) and as recently confirmed by Shankar & Ferrarese (2009). By integrating the resulting BH mass function at all times, we derive the total BH mass density $\rho_{VDF}(z)$, corresponding to BHs in the range of σ and BH mass probed by our sample at each redshift.

We then compare $\rho_{VDF}(z)$ with the BH mass density obtained by direct integration of the AGN LF $\Phi(L, z)$ from $z = 6$ up to redshift z. The latter quantity is given by

$$\rho_\bullet(>\log L_{min}, z) = \frac{1-\epsilon}{\epsilon c^2}\int_z^6 dz' \int_{\log L_{min}}^\infty \Phi(L, z') L \frac{dt}{dz'} d\log L\,. \quad (3)$$

Here ϵ represents the radiative efficiency, and for our numerical calculation, we adopt the bolometric AGN LF $\Phi(L, z)$ from SWM (using the LF from Hopkins et al. 2007 gives similar results as discussed below). At each redshift, we integrate Equation (3) above the minimum observed luminosity of $\log L_{min} = 41\,\mathrm{erg\,s^{-1}}$, although, as discussed in Section 5, the exact choice for L_{min} does not alter our conclusions.

The growth rate of an active BH of mass M_{BH} is then $\dot{M}_{BH} = M_{BH}/t_{ef}$, where the e-folding time is (Salpeter 1964)

$$t_{ef} = 4\times10^7\left[\frac{\epsilon(1-\epsilon)^{-1}}{0.1}\right]\lambda^{-1}\,\mathrm{yr}, \quad (4)$$

where λ is the ratio of the luminosity $\epsilon\dot{M}_{BH}c^2$ to the Eddington (1922) luminosity. Figure 2 compares the two independent estimates of BH mass densities. The accreted mass density at each redshift obtained from $\Phi(\sigma, z)$ and the M_{BH}–σ relation is shown with a solid curve. The solid squares show the redshifts where the mass density was computed. The long-dashed curve represents the mass density inferred from integration of the SWM AGN bolometric LF. Given that the ages of galaxies in the sample have a median associated uncertainty of $\pm$ 1 Gyr, at any time $t(z)$ the BH mass density from AGNs to be compared to $\rho_{VDF}(z)$ is systematically uncertain by the mass accreted within $t \pm 1$ Gyr, which we show as the gray area.[5] We choose a constant mean radiative efficiency of $\epsilon = 0.085$, which provides

[5] Note that the $t \pm 1$ Gyr uncertainty is for $\rho_{VDF}(z)$. However, in our calculations, assigning the uncertainty to $\rho_\bullet(z)$ or $\rho_{VDF}(z)$ makes no difference. If the time of formation of the galaxies is uncertain by $\pm$1 Gyr, then statistically the $\rho_{VDF}(z)$ at the time t can be compared with the cumulative mass accreted at any time $t \pm 1$ Gyr.

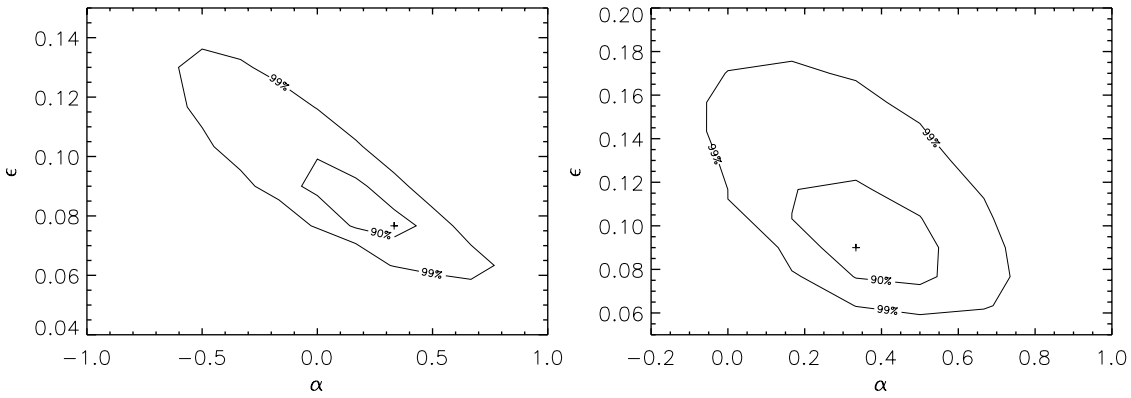

Figure 3. Confidence levels of 90% and 99% computed assuming $\chi^2 = \chi^2_{\rm min} + 2.30$ and $\chi^2 = \chi^2_{\rm min} + 9.21$, respectively, for two parameters in the model, the radiative efficiency ϵ and the exponent α, where the normalization of the $M_{\rm BH}$–σ relation evolves as $\propto (1+z)^{\alpha}$. Left panel: χ^2 computed by assuming that no correlation exists between BH mass densities computed at different redshifts. The cross marks the best-fit value of $\epsilon = 0.077$ and $\alpha = 0.33$ corresponding to the minimum $\chi^2_{\rm min} \sim 3$ (for eight degrees of freedom). Right panel: confidence levels computed inserting all the significant sources of correlations among different redshift bins. It is evident that either way a strong redshift evolution in the $M_{\rm BH}$–σ relation is ruled out at a high confidence level, if the radiative efficiency is constant in time.

a good match to the BH mass density at $z = 0$ (e.g., Haiman et al. 2004; SWM). It can immediately be inferred from the left panel, which assumes an unevolving $M_{\rm BH}$–σ relation, that $\rho_{\rm VDF}(z)$ and $\rho_\bullet(z)$ are consistent with each other within errors, and therefore a strong evolution with redshift in the $M_{\rm BH}$–σ relation is not required. Very similar results are found if we adopt the bolometric LF from Hopkins et al. (2007), shown as the dot-dashed curve in the same figure. In this case, we use a slightly higher radiative efficiency of $\epsilon \sim 0.11$ to renormalize the total $z = 0$ accreted mass density to the local value, due to the fact that the bolometric corrections used by Hopkins et al. (2007) are about 30% higher then those adopted by SWM. Nevertheless, even in this case we find that $\rho_\bullet(z)$ well matches $\rho_{\rm VDF}(z)$ at all times.

Joint confidence levels on the two parameters ϵ and α, inferred from a χ^2 analysis are shown in Figure 3. The cross marks the best-fit model with $\epsilon = 0.077$ and $\alpha = 0.33$ (corresponding to the minimum $\chi^2_{\rm min} \sim 3$ for eight degrees of freedom), which is shown in the right panel of Figure 2. Once a constant radiative efficiency is fixed to match the $z = 0$ local and accreted mass densities, it is evident that the available data favor a relatively mild redshift evolution of the $M_{\rm BH}$–σ relation with $\alpha \lesssim 0.3$, while a strong evolution with $\alpha \gtrsim 1.3$ is ruled out at more than 99% confidence level. Likewise, negative evolution with $\alpha \lesssim -1$ is ruled out for any choice of ϵ. We also note that values of $\alpha \gtrsim 1$ yield the unphysical result that the absolute total BH mass density *increases* from $z = 0$ to $z \gtrsim 0.7$, as shown in Figure 4. The confidence levels in Figure 3 have been computed by assuming that the BH mass densities $\rho_{\rm VDF}(z)$ computed at different redshifts to be independent of one another. This may be an oversimplification given that the VDF computed at any given redshift depends directly on the VDF at $z = 0$. We therefore repeat the full χ^2 analysis by computing the full covariance matrix COV$[\Delta\rho_{\rm VDF}(z_i), \Delta\rho_{\rm VDF}(z_j)]$. The details of how we compute the variances and covariances are given in the Appendix. Here we point out that the χ^2 computed by switching to the full covariance matrix yields very similar, if not stronger, results. We still find, in fact, a best-fit value of $\alpha \sim 0.33$, with a χ^2 per degree of freedom of 0.77, with high values of $\alpha \gtrsim 1.0$ excluded at more than 99% confidence level, and a value of $\alpha \sim 0$ only marginally acceptable.

It is clear from Equation (3) that the accreted BH mass density does not depend on the assumed duty cycle or Eddington-ratio distribution $\lambda(M_{\rm BH},z)$, apart from a weak dependence

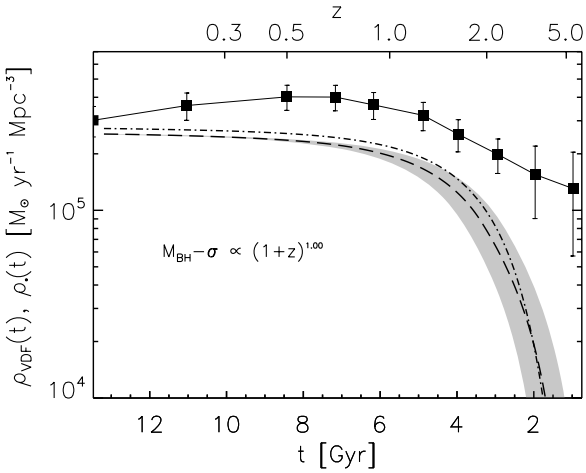

Figure 4. Same format as Figure 2, with parameters $\alpha = 1$ and $\epsilon \sim 0.08, 0.10$ for the SWM and Hopkins et al. (2007) LFs, respectively.

on the latter through the lower limit of the integration. The strongest dependences are on the radiative efficiency and on the bolometric corrections (see also Figure 9 in SWM). On the other hand, the Eddington-ratio distribution and its evolution with redshift can be constrained by comparing the AGN-based and VDF(z)-based differential BH mass functions (rather than comparing only the integrated quantities). The $\Phi(\sigma, z)$ convolved with the $M_{\rm BH}$–σ relation (Equation (2)), in fact, predicts the shape of the BH mass function for $M_{\rm BH} \gtrsim M_{\rm BH,min}$. On the other hand, as extensively discussed in the literature (see SWM, and related work by, e.g., Cavaliere et al. 1982; Small & Blandford 1992; Salucci et al. 1999; Yu & Tremaine 2002; Marconi et al. 2004; Shankar et al. 2004), if a mean Eddington ratio $\lambda = L/L_{\rm Edd}$ is assumed for the active BHs, then through a continuity equation and an assumed initial condition, the AGN LF can be directly mapped into a BH mass function at all times. The "break" in the predicted BH mass function will then approximately reflect the break $L^*(z)$ in the observed AGN LF, i.e., $M_{\rm BH}{}^*(z) \propto L^*/\bar{\lambda}$, where $\bar{\lambda}$ is the mean Eddington ratio. Following Sołtan (1982) and Salucci et al. (1999), SWM (see also, e.g., Yu & Tremaine 2002) showed that constraints on the mean radiative efficiency and Eddington ratio of BHs can be gained by comparing the directly measured and the accreted BH mass functions. However, the BH mass function

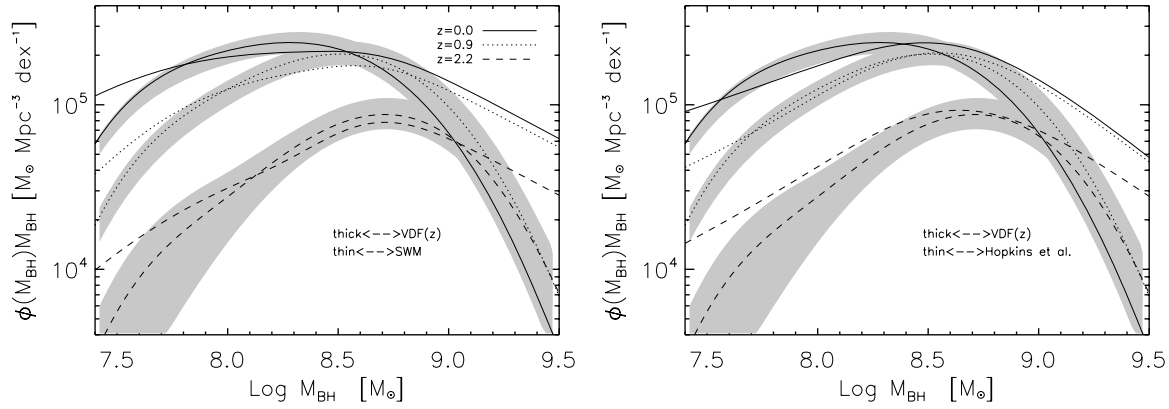

Figure 5. Comparison between the mass functions predicted from $\Phi(\sigma, z)$ convolved with the M_{BH}–σ relation whose normalization evolves as $\propto (1+z)^{0.33}$ (thick curves, with the uncertainty shown shaded in gray), and the mass function predicted from the AGN LFs of Shankar et al. (2009; left panel) and Hopkins et al. (2007; right panel). A constant Eddington ratio of $\lambda = 0.6, 1.0$ has been assumed for computing the accreted mass functions in the left and right panels, respectively. It can be seen that the choice of a single constant Eddington ratio provides a good match to the velocity dispersion-based BH mass functions, at least around the peak of the distributions. A good match is also found extending the comparison up to $z \gtrsim 3$; however, the large uncertainties at these redshifts prevent any firm conclusion.

has directly been measured only locally, so this comparison can be performed only at $z = 0$, and cannot be used to glean information on the evolution of these two parameters.

The left panel of Figure 5 compares the BH mass function predicted from the combination of $\Phi(\sigma, z)$ and the mildly evolving best-fit M_{BH}–σ relation with a normalization $\propto (1+z)^{0.33}$ (shown as thick curves, with their uncertainty shown in gray), and the mass function predicted from the AGN LF of SWM assuming a mean $\bar{\lambda} = 0.6$ (shown as thin curves).[6]

Figure 5 shows that up to $z \lesssim 3$, a *constant* (nonevolving) mean Eddington ratio of $\bar{\lambda} = 0.6$ provides a good match between the shapes of the accreted BH mass function and that computed from the VDF. At the low-mass end, the VDF-based BH mass function starts being incomplete, while at the high-mass end, a higher intrinsic scatter in the M_{BH}–σ relation and/or a more complicated Eddington-ratio distribution may improve the match. Fully matching the two BH mass functions is beyond the scope of this paper (see SWM for further analysis). Our aim here is merely to demonstrate that our simple approach also provides hints on the mean Eddington ratio and its redshift evolution. Similar results are found switching to the Hopkins et al. (2007) LF. The right panel of Figure 5 shows that a good match between the BH mass functions is recovered on adopting a constant $\lambda = 1.0$. Although systematic uncertainties in the bolometric AGN LF preclude tighter constraints on the mean Eddington ratio (see SWM for further discussions on these issues), it is remarkable that simple models with $0.5 \lesssim \lambda \lesssim 1.0$ constant with redshift can provide a reasonable match with the VDF-based BH mass functions. An independent way to constrain the Eddington-ratio distribution and its evolution with redshift can be derived by matching the halo clustering implied by the redshift dependent model BH mass function and the observed AGN clustering (Shankar et al. 2008; F. Shankar et al. 2009, in preparation). We have also checked that the same values of λ provide a good match even at $z \gtrsim 3$; however, the large uncertainties associated with the VDF at these high redshifts prevent any firm conclusion.

A somewhat different version of the above exercise was performed by Haiman et al. (2007). Under the assumption that the duty cycle of quasar activity is short, Haiman et al. (2007) matched the instantaneous quasar LF at each redshift to the LF predicted from $\rho_{VDF}(z)$, plus an assumed constant (nonevolving) duty-cycle and Eddington-ratio distribution. This approach neglects the BH mass accreted during the luminous quasar phases (or at least any corresponding variation of the "quasar light-curve" caused by the growth in BH mass), and places a constraint directly on the relation between quasar luminosity L and host velocity dispersion σ. While the L–σ relation is essentially a convolution of the Eddington-ratio distribution with the M_{BH}–σ relation, this approach cannot be used to study these two relations separately. Nevertheless, Haiman et al. (2007) found no evidence for any evolution in the L–σ relation with redshift; their fits to the quasar LF are consistent with a constant $0.3 \lesssim \bar{\lambda} \lesssim 0.5$ combined with a nonevolving M_{BH}–σ relation. Since the M_{BH}–σ relation is indeed found here, independently, to be nonevolving, this breaks the degeneracy in the result of Haiman et al. (2007) and also requires that the evolution in the Eddington-ratio distribution be modest.

4. DISCUSSIONS

4.1. Varying the Model Assumptions

We have studied more complicated scenarios where we also allow for the scatter and/or the slope of the M_{BH}–σ relation to increase with redshift. For example, steadily increasing the slope from 3.83 to, say, 5.5, at a fixed scatter of 0.22 dex, still implies $\alpha \sim 0.35$. The left panel of Figure 6 shows instead the comparison between the $\rho_\bullet(z)$ and the $\rho_{VDF}(z)$, assuming that the scatter increases with redshift from $\eta = 0.22$ at $z = 0$ to $\eta = 0.40$ at $z = 5.7$, the highest redshifts probed by our sample. It can be seen that the best-fit model requires $\alpha = 0.15$, even lower than what reported in Figure 2. This is expected as these models tend to increase the BH mass density associated with the VDF at a given redshift, implying an even milder degree of evolution in the M_{BH}–σ normalization. The right panel of Figure 6 compares the implied mass functions predicted by the same $\eta(z)$-model and by the AGN LF. Similarly to the best-fit model discussed in Section 3, a good match can be recovered assuming a constant $\lambda = 0.6$. Moreover, steadily increasing the intrinsic scatter from 0.22 to 0.4 dex significantly improves the match between the VDF- and AGN-based BH mass functions at both the high- and low-mass ends. Increasing the in-

[6] Note that we assumed an initial duty cycle of 0.5 at $z = 6$; however, the BH mass function at $z \lesssim 3.5$ becomes independent of this assumption. See SWM for further details.

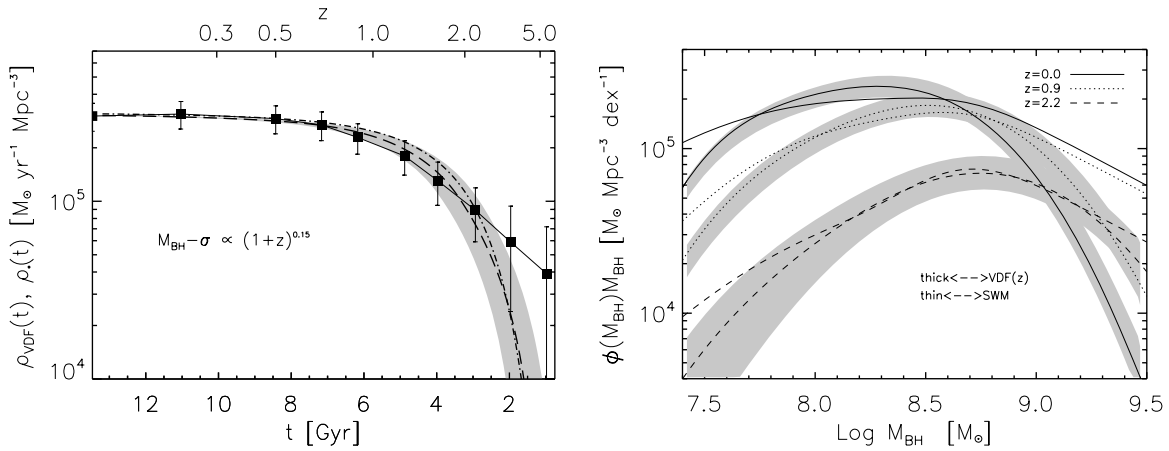

Figure 6. Left panel: comparison between the $\rho_\bullet(z)$ and the $\rho_{\rm VDF}(z)$ computed for a model in which the $\Phi(\sigma, z)$ is convolved with a $M_{\rm BH}$–σ relation the scatter of which increases with redshift from $\eta = 0.22$ to 0.40. Right panel: comparison between the mass functions predicted from the same model and from the AGN LFs with $\lambda = 0.6$.

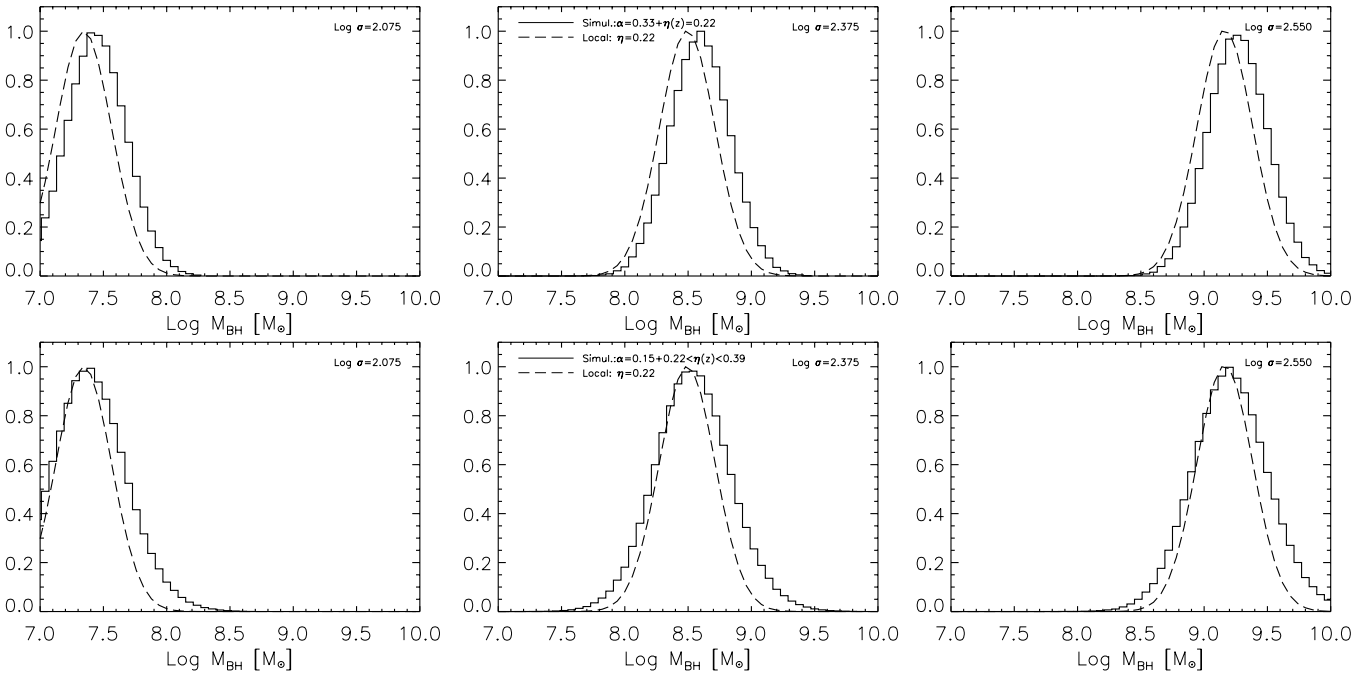

Figure 7. In each panel the solid histograms show the mean of a set of Monte Carlo simulations which compute from our models the expected distribution of BH masses at fixed velocity dispersion, as labeled (see the text for details). The long-dashed lines refer to the Gaussian distribution with $\eta = 0.22$ measured by Tundo et al. (2007). Both our models with constant (upper panels) or evolving (lower panels) scatter still produce at $z = 0$ BH mass distributions at fixed velocity dispersion comparable to what is observed. Models characterized by stronger redshift evolution will then evidently predict a scatter in the local $M_{\rm BH}$–σ relation much larger than what is observed.

trinsic scatter in the distribution may be analog to allowing the $M_{\rm BH}$–σ relation to steadily increase with increasing redshift only in the most massive BHs in the distribution (those with MBH $\gtrsim 10^9\,M_\odot$) at each redshift. However, the $M_{\rm BH}$–σ related to the bulk of the BH population should not evolve much.

We have also explored different models for the redshift evolution in the $M_{\rm BH}$–σ relation. For example, a model in which a quadratic term of the type $\delta \times \log(1+z)^2$ is added in Equation (2) (see Wyithe 2004 for a similar test applied to the local $M_{\rm BH}$–σ relation), produces a good match between $\rho_{\rm VDF}(z)$ and $\rho_\bullet(z)$ if $\alpha \sim \delta \sim 0.1$, with $\chi^2 \sim 4$, comparable to our best-fit model. We therefore conclude that although the choice for the redshift evolution model in Equation (2) is not unique, alternative solutions will still provide similar constraints on the net amount of allowed evolution.

4.2. The Scatter in the M_{BH}–σ Relation

At each redshift, our approach assumes that new BHs are formed with a mass that is tightly imposed by the velocity dispersion of the host galaxy. Increasing the normalization and/or scatter of the $M_{\rm BH}$–σ relation at high redshift therefore induces in the local universe a finite spread in BH mass at fixed velocity dispersion. If the evolution is steep, this can exceed the observed scatter $\eta \lesssim 0.22$ dex. Each panel in Figure 7 plots as solid lines the median BH mass distribution of 100 Monte Carlo simulations corresponding to a given bin of velocity dispersion, as labeled. The BH masses are derived from the redshift-dependent $M_{\rm BH}$–σ relation where the redshifts are randomly extracted from the age distribution $p_{ij}(\sigma)$ competing to each velocity dispersion. The long-dashed lines refer to the Gaussian distribution with $\eta = 0.22$ measured by Tundo et al. (2007).

Both our models with constant (upper panels) or evolving (lower panels) scatter still produce at $z = 0$ BH mass distributions at fixed velocity dispersion comparable to what is observed. The small off-set in the Gaussian distributions predicted by our simulations with respect to those observed is induced by the sampling of higher redshift, more massive BHs. Models characterized by stronger redshift evolution with $\alpha \gtrsim 0.4$ will then evidently predict a scatter in the local $M_{\rm BH}$–σ relation much larger than what is actually observed. Mergers are then required to be a significant component in the evolution of the BH population in these models, as the Monte Carlo simulations performed by Peng (2007) show that random BH mergers will tighten the relations between BH and host galaxy masses at late times. However, frequent mergers may, on the other hand, predict too many massive BHs with respect to those seen in the local universe (see Figure 13 in SWM).

4.3. Systematic Uncertainties in the Method

The main result of this paper is shown in the right panel of Figure 2, which demonstrates that a good match between $\rho_{\rm VDF}(z)$ and $\rho_\bullet(z)$, can be achieved by assuming a mild redshift evolution in the $M_{\rm BH}$–σ relation with $\alpha \lesssim 0.3$. These results are based on the age distributions p_{ji} derived from Bernardi et al. (2006). However, MOPED-based galaxy ages are, on average, larger at fixed velocity dispersion, predicting a flatter dependence $\Phi(\sigma, z)$ as a function of redshift z (see Figure 1). This will correspondingly flatten $\rho_{\rm VDF}(z)$ versus redshift, and decrease the best-fit α, therefore requiring an even milder redshift evolution in the $M_{\rm BH}$–σ relation. A null evolution in the $M_{\rm BH}$–σ relation is expected in basic AGN feedback models (e.g., Silk & Rees 1998), in which a tight correlation derives by imposing equilibrium between the energy released by the central BH and the gas binding energy, linked to the velocity dispersion.

Bernardi et al. (2007), Graham (2007), and Shankar & Ferrarese (2009) have discussed selection biases in the available sample of BHs that may induce systematic uncertainties in the determination of the local BH mass function. However, our conclusions are not affected by these uncertainties, because a change in the local BH mass density would be absorbed in the radiative efficiency ϵ (i.e., ϵ would be modified, to match $\rho_{\rm VDF}(z)$ and $\rho_\bullet(z)$ at $z = 0$, but α would not change). By the same token, our results are only weakly dependent on whether or not the bulges of spirals are included in the estimate of the local BH mass function (a weak dependence arises only because the addition of the spiral bulges slightly skews the age distribution of the total population to younger ages; this becomes increasingly less important toward higher redshifts, where a progressively smaller fraction of the total BH mass density is contributed by the low-σ galaxies).

Likewise, uncertainties in redshift-independent bolometric corrections do not alter our conclusions. The bolometric correction adopted in SWM is lower by ∼30% with respect to that used by Hopkins et al. (2007), but the sole effect of this difference is to yield a proportionally smaller value of the mean radiative efficiency to recover the match between $\rho_{\rm VDF}(z)$ and $\rho_\bullet(z)$ at $z = 0$ (see left panel of Figure 2). Moreover, the break luminosity and bright-end slopes of the SWM and Hopkins et al. (2007) LFs are somewhat different (see Figure 4 in SWM). Nevertheless, within uncertainties, the resulting BH accretion histories obtained from the two LFs have a similar behavior with redshift, both placing the same constraint $\alpha \lesssim 0.35$ for the evolution in the normalization of the $M_{\rm BH}$–σ relation.

On similar grounds, if we assume that the BHs in our sample radiate at even lower luminosities than the $L_{\rm min}$ considered in the integral of Equation (3), our results do not change. For example, lowering the minimum luminosity to $\log L_{\rm min}/{\rm erg\,s^{-1}} = 40$, the cumulative emissivity of AGNs increases by about $\sim 20\%$ at all redshifts yielding a very similar behavior with time. We have checked that a proportionally higher radiative efficiency and similar values of α plugged into Equation (3) keeps the good match with the $\rho_{\rm VDF}(z)$.

Our conclusions about the (lack of) evolution in the normalization of the $M_{\rm BH}$–σ relation, in general, are more dependent on redshift-dependent effects. For example, if the bolometric correction increased to high z (or, e.g., if obscuration were more significant at higher redshift), this would again further decrease our favored mild positive redshift evolution in the $M_{\rm BH}$–σ normalization. Likewise, evolution in the mean radiative efficiency and/or the assumed scatter in the $M_{\rm BH}$–σ relation would modify our results, in the sense that our predicted evolution would be milder if either increased toward high z. In principle, to allow for a stronger evolution in the $M_{\rm BH}$–σ relation the radiative efficiency must significantly decrease at $z \gtrsim 3$ to boost the accreted mass density at fixed AGN luminous density. However, we have checked that ϵ must then rapidly increase at lower redshifts in order not to overproduce the local BH mass density. More quantitatively, if we set $\epsilon \sim 0.05$ at $z \gtrsim 3$, then it must be that $\epsilon \gtrsim 0.05 \times [7/(1+z)]^{0.5}$ at lower redshifts. Such an evolution in ϵ is not enough to allow for a strong variation in the $M_{\rm BH}$–σ relation. We found that $\rho_{\rm VDF}(z)$ can match the $\rho_\bullet(z)$ implied by the $\epsilon(z)$-model if $\alpha \sim 0.3$, which is close to our best-fit model. On other grounds, as recently shown by Shankar et al. (2008), a too low radiative efficiency at high redshifts seems to be disfavored by BH accretion models which simultaneously reproduce the strong quasar clustering measured at $z = 3$–4 in Sloan Digital Sky Survey (SDSS) by Shen et al. (2007), the mean Eddington ratio of $\lambda \gtrsim 0.5$, measured by Shen et al. (2008) for the same quasar sample, and the high redshift quasar LF (e.g., Richards et al. 2006; Fontanot et al. 2007; Shankar & Mathur 2007).

4.4. Evolving the Magorrian Relation

Most of the results from other groups discussed in Section 1 focus on the ratio between BH mass and stellar *mass*. The latter may settle on longer timescales with respect to the galaxy velocity dispersion, the amplitude of which is linked to the central potential well which grows faster than the overall evolution of the halo (Zhao et al. 2003). In order to get some hints on the actual evolution of the $M_{\rm BH}$–$M_{\rm STAR}$ relation with redshift, we have converted the galaxy stellar mass function into a BH mass function assuming the $M_{\rm BH}$–$M_{\rm STAR}$ ratio evolving as $(1 + z)^\zeta$. We have used the recent near-infrared stellar mass function by Pérez-González et al. (2008), well constrained within $0 \lesssim z \lesssim 3$ and $10 \lesssim \log M_\star/M_\odot \lesssim 12$. We have then converted the latter into a BH mass function by assuming that, on average, about $0.7 \times 10^{-3}(1+z)^\zeta$ (e.g., Magorrian et al. 1998; Marconi & Hunt 2003) of the total stellar mass is locked up in spheroids and is associated with the central BH, with a Gaussian scatter around the mean of 0.3 dex (e.g., Häring & Rix 2004). In this case, we find that $\zeta \lesssim 0.3$ is a necessary condition for the BH mass density to be consistent with the accreted mass from AGNs, the latter derived assuming a fixed value of the radiative efficiency. This result is in agreement with the degree of evolution discussed in Section 3 found by evolving the $M_{\rm BH}$–σ relation. Although these results are in reasonable agreement with other works (Marconi et al. 2004; Merloni et al. 2005; De

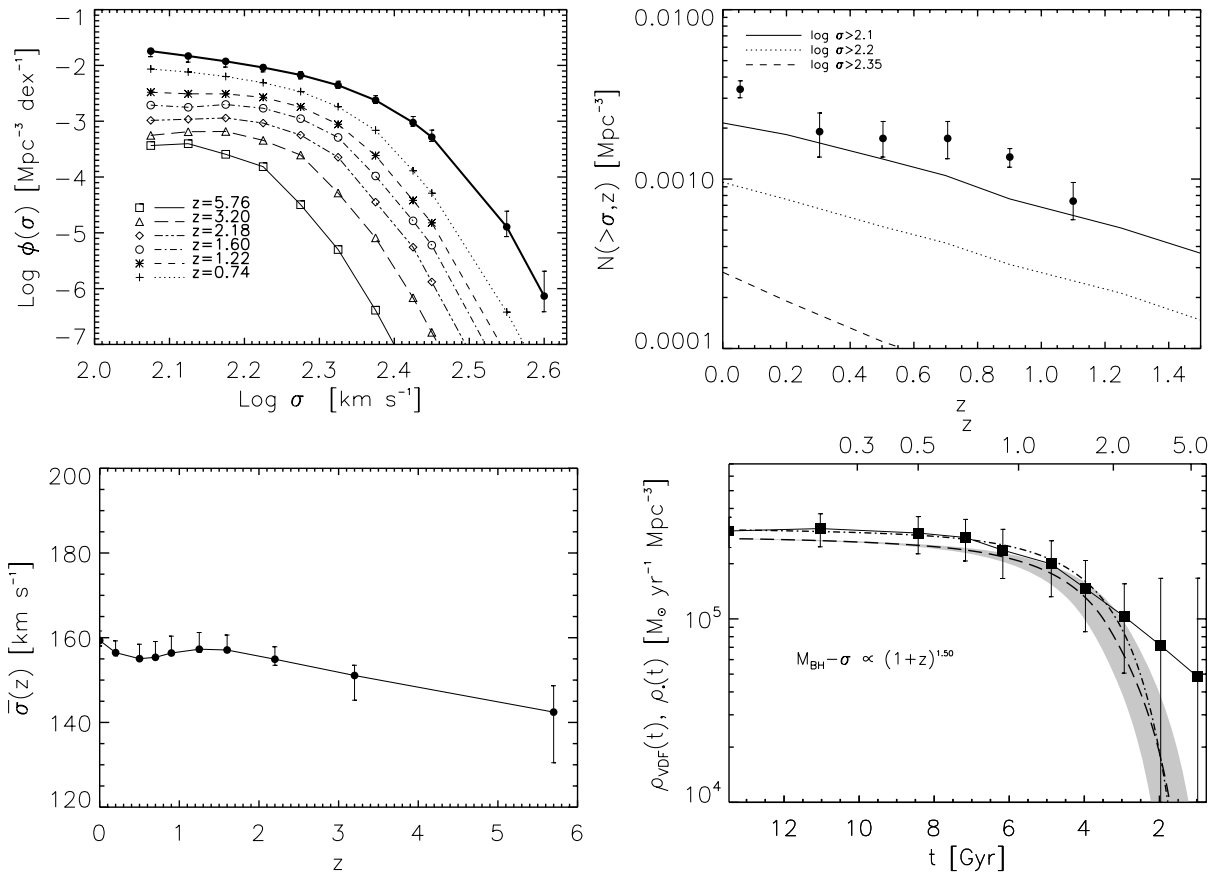

Figure 8. Results for a model in which we allow the mean galaxy velocity dispersion to decrease at higher redshifts to mimic the effects of prolonged wet activity in the host galaxies since their formation epoch. We assume an evolution of the type $\sigma(z) = \sigma(0) \times (1+z)^{-\gamma}$ with $\gamma = 0.25$. The downsizing effect is canceled out (upper left) and the match with DEEP2 number density evolution is significantly worsen (upper right). At variance with our previous results this model predicts a mean velocity dispersion about flat out to $z \sim 2$ (lower left) and, more important, a good match between $\rho_{\rm VDF}(z)$ and $\rho_\bullet(z)$ with $\alpha = 1.5$ (lower right).

Zotti et al. 2006; SWM; Merloni & Heinz 2008), uncertainties on the lower limit of the stellar mass function and/or on the true fraction of stellar mass associated with BH growth at any time, make this method less reliable than the one based on velocity dispersion, and we therefore do not pursue it further.

4.5. The Impact of Mergers

So far we have neglected mergers in our calculations. Major mergers between massive galaxies do occur, although recent work has suggested that the galaxy merger rate may be lower than previously thought. Drory & Alvarez (2008) compared the time variation in the stellar mass function with the evolution implied by the star formation rate alone, concluding that galaxies with stellar masses above $10^{11}\,M_\odot$ undergo at most one major merger since $z \sim 1.5$, in agreement with the results of Bell et al. (2007). Lotz et al. (2008) find evidence for an even lower merger rate since $z \sim 1$ from the DEEP2 survey. Most importantly, however, a significant rate of major mergers would strengthen our conclusions. In velocity dispersion space, collisionless major mergers do not significantly affect the final σ. For example, in a dry merger of comparable-mass galaxies with mass M_1 and M_2, and corresponding velocity dispersions σ_1 and σ_2, the resulting galaxy will have a velocity dispersion $\sigma^2 \sim \left[M_1\sigma_1^2 + M_2\sigma_2^2\right]/(M_1+M_2) \lesssim \max\left(\sigma_1^2, \sigma_2^2\right)$ (e.g., Ciotti et al. 2007). Therefore, if the masses of the two galaxies are comparable, the final σ will be close to the velocity dispersion of the progenitors.

Dry mergers would then double the number of galaxies we predict at fixed σ. Every dry major merger would in fact "split" the galaxy into two (going back in time), adding an extra galaxy with the same σ, compared to our present predictions (which neglect mergers). In turn, this implies that the merger-free VDF $\Phi(\sigma, z)$ computed above for $z > 0$ is a *lower* limit to the true abundance of galaxies with velocity dispersion σ at redshift z. The associated BH mass density $\rho_\bullet(z)$ will consequently also be underestimated at redshift z. The inclusion of any mergers then predicts a larger BH mass density at fixed σ; to compensate for this increase, a lower normalization of the $M_{\rm BH}$–σ relation at $z = 1-2$ is then required, which strengthens our conclusions that large α values are excluded by the match between $\rho_{\rm VDF}(z)$ and $\rho_\bullet(z)$ (see the left panel in Figure 2).

However, if dissipation played a nonnegligible role during the evolution of the galaxy (either as a result of mergers, or in isolation), then the velocity dispersion may increase with time from the epoch of first collapse. To mimic such effects, we allow all velocity dispersions to increase at higher redshifts as $\sigma(z) = \sigma(0) \times (1+z)^{-\gamma}$. Most probably this evolution is mass and/or velocity-dependent, nevertheless this approach will be able to set interesting constraints on the mean variation of σ. Also, any estimate for γ should here be considered as a lower limit to the actual evolution of σ, as we neglect the still poorly understood increase in galaxy number density due to possible galaxy mergers. In Figure 8, we show the main results for a model with $\gamma = 0.25$ and $\alpha = 1.5$. Note that with the adopted scaling $M_{\rm BH} \propto \sigma^\beta$ with $\beta \approx 4$, we expect a degeneracy between γ and α given approximately by $\gamma \approx \alpha/\beta \approx \alpha/4$ (although the degeneracy is modified slightly by the assumed scatter and age spread of BHs at a given z and σ). We find that the downsizing

evolution in this case is canceled out (upper left panel), as all galaxies are now pushed to lower and lower σ at higher redshifts.

The evolving number density in this model, shown in the upper-right panel of Figure 8, seems to be at variance with the number density evolution of early-type galaxies within $0 \lesssim z \lesssim 1$ inferred from DEEP2 by Faber et al. (2007; solid points in the same figure). However, lacking a clear understanding of how $\Phi(\sigma, z)$ should evolve in the presence of mergers, this model cannot be ruled out, although some inconsistencies can already be pointed out. From the figure it can be seen that the number density of the massive red galaxies in DEEP2 at the intermediated redshifts of $0.5 < z < 1$ should be matched with galaxies characterized by a velocity dispersion of $\sigma \lesssim 100\,\mathrm{km\,s^{-1}}$. Alternatively, the DEEP2 number densities could be matched with the number density of galaxies with larger velocity dispersions if mergers were a significant component in the evolution of these galaxies, thus significantly increasing their number density at higher redshifts. However, the latter hypothesis may contradict independent results (e.g., Lotz et al. 2008). The dissipative model described here also predicts a mean velocity dispersion about flat out to $z \sim 2$ and slightly decreasing at higher redshifts, as shown in the lower left panel of Figure 8.

The main achievement of this model is the good match between $\rho_{VDF}(z)$ and $\rho_\bullet(z)$ even if a strong evolution in the M_{BH}–σ relation has been assumed ($\alpha = 1.5$), as shown in the lower right panel of Figure 8. This model is characterized by a significant dissipative phase in the evolution of typical early-type galaxies, which could represent an interesting constraint for galaxy evolution models, and it can in principle be tested through hydrodynamical simulations.

On the other hand, a major problem with the dissipative model is represented by its implied Eddington-ratio distribution. We in fact find that the strong increase in the M_{BH}–σ normalization at higher redshifts requires a significant *decrease*, by up to a factor of a few, in the mean Eddington ratio $\bar{\lambda}(z)$ to keep the match between the BH mass functions at $z \gtrsim 2$ shown in Figure 5. The latter behavior of $\bar{\lambda}(z)$ is at variance with several works which actually claim an almost constant or probably increasing $\bar{\lambda}(z)$ at higher redshifts (e.g., McLure & Dunlop 2004; Shankar et al. 2004; Vestergaard 2004; Kollmeier et al. 2006; Netzer & Trakhtenbrot 2007; SWM; Shen et al. 2008b; Shankar et al. 2009).

4.6. Comparison with Previous Works

The relatively mild M_{BH}–σ redshift evolution inferred from our approach may seem in apparent disagreement with some recent independent studies. As briefly mentioned in Section 1, Treu et al. (2007) and Woo et al. (2008) have randomly compiled from the SDSS Data Release 4 a sample of about 20 Seyferts galaxies in the redshift range $0.37 \lesssim z \lesssim 0.57$. Their results, shown as open circles in Figure 9, are compared with those of Shen et al. (2008a, shown as filled circles), who estimated the M_{BH}–σ relation for a larger sample of active galaxies up to $z = 0.452$. While the latter claim that no significant evolution in the M_{BH}–σ relation is detectable from their sample, Woo et al. (2008) confirm the results by Treu et al. (2007) that a significant increase of ~ 0.2 dex in BH mass at fixed velocity dispersion must occur within $z = 0$ and $z \sim 0.5$. Our best-fit model, shown at redshifts $z = 0$ and $z = 0.5$ with long-dashed and solid lines respectively, shows no strong evolution within this redshift range and it is in reasonable agreement with both samples. A significant discrepancy is noticeable with

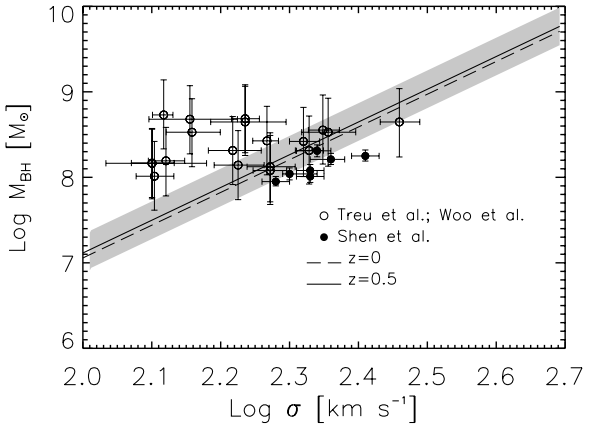

Figure 9. Our best-fit model for the M_{BH}–σ relation is plotted at $z = 0$ and $z = 0.5$, as labeled, and compared with recent data from Treu et al. (2007) and Woo et al. (2008), shown with open symbols, and Shen et al. (2008a), shown with filled symbols.

respect to the Woo et al. (2008) results for velocity dispersions $\log(\sigma/\mathrm{km\,s^{-1}}) \lesssim 2.3$. However, systematic uncertainties may affect these estimates; for example, as also discussed by Woo et al. (2008), especially in galaxies with lower BH mass, the host galaxy contribution to the 5100 Å luminosity may lead to an overestimation of the true BH mass. Overall, given the systematics and biases which affect these kind of studies (e.g., Lauer et al. 2007), we do not find strong evidence for a disagreement between these works and our results. For the same reasons, we do not attempt comparisons with the results obtained from higher redshift studies.

Merloni et al. (2004) compared the accreted BH mass density in AGNs with the cosmological global star formation rate density (see also Haiman et al. 2004). Although their conclusions depend on additional assumptions about the fraction of the star forming galaxies which are linked to BH growth at a given redshift, irrespective of the adopted value of the radiative efficiency their best-fit relation yields $\alpha \approx 0.5$, somewhat higher, but still consistent, with the value found here, and they also rule out $\alpha \gtrsim 1.2$ at a high confidence level. Hopkins et al. (2006) also describe a model-independent integral constraint that defines an upper limit to the allowed degree of evolution in the ratio of BH mass to host galaxy luminosity or mass, as a function of redshift. By comparing the AGN density with the luminosity and mass functions in different bands from redshifts $z = 0$–2, they rule out at $\gtrsim 6\sigma$ a BH–host galaxy mass ratio significantly larger at high redshifts than locally. Cattaneo & Bernardi (2003) combined a relation between mean age and velocity dispersion, derived from a sample of SDSS local early-type galaxies, with the Sheth et al. (2003) local VDF. By assuming a redshift-independent mean Eddington ratio, radiative efficiency and obscuration correction, they were then able to reproduce the AGN optical and X-ray LFs. As mentioned above, similar calculations have been performed recently by Haiman et al. (2007), whose results imply, assuming a nonevolving M_{BH}–σ relation, that in order to reproduce the bolometric quasar LF, the quasars must shine at a mean sub-Eddington regime of $\lambda = 0.5$ that is approximately constant with time. This conclusion was confirmed by the independent estimates of SWM. However, the works by Cattaneo & Bernardi (2003); Haiman et al. (2007) can only constrain the *combination* of the Eddington-ratio distribution and the M_{BH}–σ relation,

while our approach here can simultaneously constrain the mean accretion histories of BHs and their host galaxies, and the mean Eddington ratio of BHs at all times. A further difference is that the analysis of Haiman et al. (2007) can constrain the quasar lifetime, while the results here rely on the comparison between time-integrated quantities, and are strictly independent of the quasar lifetime.

5. CONCLUSIONS

In this work we combined the local VDF with the stellar age distributions estimated by Bernardi et al. (2006), to compute the VDF at higher redshifts, $\Phi(\sigma, z)$. In agreement with previous work, we find statistical evidence for downsizing, whereby the stellar populations in galaxies with higher velocity dispersions formed earlier, irrespective of the specific model we adopt for computing the galactic ages. We then computed the BH mass function associated with $\Phi(\sigma, z)$ at each redshift z, through a BH mass–velocity dispersion relation whose normalization was allowed to evolve with redshift as $\propto (1+z)^{\alpha}$. Our main underlying assumptions are that most of the growth of the central BH occurs simultaneously (within $\pm$ 1 Gyr) with the formation of the host's potential well, and that the measured stellar ages represent this formation time to within a similar accuracy. The BH mass density $\rho_{\rm VDF}(z)$ inferred from the VDF can then be compared with the accumulated BH mass density implied by the time integral of the AGN LF, $\rho_{\bullet}(z)$. We find significant evidence that the match between $\rho_{\rm VDF}(z)$ and $\rho_{\bullet}(z)$ implies a relatively mild redshift evolution, with $\alpha \lesssim 0.35$, and with values of $\alpha \gtrsim 1.3$ excluded at more than 99% confidence, although a possible stronger evolution for the more massive BHs may still be allowed. If a positive redshift evolution stronger than $\alpha \gtrsim 1$ were to be confirmed independently in the future, then this would be a robust indication that dissipative processes played a significant role in galaxy evolution, resulting in an increase in the velocity dispersion of the spheroid components of individual galaxies with cosmic time. However, we also find evidence that a dissipative model predicts a mean Eddington ratio decreasing with increasing redshift, at variance with several independent studies.

This work was supported by NASA grants NNG05GH77G (to FS), NNG04GI88G and NNX08AH35G (to ZH), and LTSA-NNG06GC19G (to MB). Z.H. also acknowledges support by the Polányi Program of the Hungarian National Office of Technology. F.S. thanks David H. Weinberg for interesting discussions and Andrew Gould for significant contributions to the statistical analysis.

APPENDIX

THE COVARIANCE IN THE REDSHIFT EVOLUTION OF THE BLACK HOLE MASS DENSITY

Here, we describe in some detail how we built the covariance matrix which expresses the relative errors between any two BH mass density estimates at two different redshifts. The covariance we describe here originates from the simple fact that the BH mass density accumulates with time, so that variations in $\rho_{\rm VDF}(z)$ in neighboring redshift bins will be necessarily correlated. This will affect the χ^2 we compute (see Equation (A9)). We ignore all other sources of covariance.

In discrete form, we can express the BH mass density $\rho_{\rm VDF}(\bar{z})$ at a given redshift $\bar{z}$ as

$$\rho_{\rm VDF}(\bar{z}) = \sum_k \delta_{\rm BH} M_{\rm BH,k} \times \left[\left(\sum_j \delta_\sigma W(\bar{z}, M_{\rm BH,k}, \sigma_j) \phi(\sigma_j) \sum_{z>\bar{z}} p_z(\sigma_j) \right) \right], \quad \text{(A1)}$$

where $\delta_{\rm x} = d\log x$, W is the Gaussian weight at redshift $\bar{z}$ (which contains the assumed redshift-dependent $M_{\rm BH}$–σ relation) used to covert the VDF $\phi(\sigma, \bar{z})$ into a BH mass function $\phi(M_{\rm BH}, \bar{z})$ at the same redshift, and where we have expressed the VDF at redshift $\bar{z}$ in terms of the local VDF at $z = 0$ via Equation (1):

$$\phi(\sigma_j, \bar{z}) = \phi(\sigma_j) \left(1 - \sum_{z<\bar{z}} p_z(\sigma_j) \right) = \phi(\sigma_j) \sum_{z>\bar{z}} p_z(\sigma_j) . \quad \text{(A2)}$$

For clarity purposes, in the following we will omit the $\delta_{\rm x}$ symbols although they are meant to be present in each summation.

Using the symbol Δ to indicate the overall uncertainty associated with a given mass density, the elements C_{ij} in the covariance matrix can then be written as

$$C_{ij} = {\rm COV}(\Delta\rho_{\rm VDF}(z_i), \Delta\rho_{\rm VDF}(z_j)) , \quad \text{(A3)}$$

which explicitly reads as

$$C_{ij} = \sum_k M^2_{\rm BH,k} \left\{ \left[\sum_j W(z_i, M_{\rm BH,k}, \sigma_j) W(z_j, M_{\rm BH,k}, \sigma_j) \times {\rm COV} \left(\Delta \left(\phi(\sigma_j) \sum_{z>z_i} p_z(\sigma_j) \right), \times \Delta \left(\phi(\sigma_j) \sum_{z>z_j} p_z(\sigma_j) \right) \right) \right] \right\} , \quad \text{(A4)}$$

where we made use of the summation and product properties of covariances (see Gould 2003), and where we considered negligible in the covariance any correlation between bins of different BH mass and/or velocity dispersion. Therefore, the full covariance matrix reduces to a double matrix summation first over all velocity dispersions then over all BH masses, each weighted by the appropriate Ws.

Through error propagation the uncertainty in the product of VDF and age distributions can be expressed as

$$\Delta \left(\phi(\sigma_j) \sum_{z>z_i} p_z(\sigma_j) \right) = \Delta(\phi(\sigma_j)) \sum_{z>z_i} p_z(\sigma_j) + \phi(\sigma_j) \sum_{z>z_i} \Delta(p_z(\sigma_j)) . \quad \text{(A5)}$$

By plugging Equation (A5) into Equation (A4) we can now write the covariance matrix relative to a single bin σ_j as

$$\begin{aligned}\mathrm{COV}&\left(\Delta\left(\phi(\sigma_j)\sum_{z>z_i}p_z(\sigma_j)\right),\Delta\left(\phi(\sigma_j)\sum_{z>z_j}p_z(\sigma_j)\right)\right)\\&=\Delta^2(\phi(\sigma_j))\sum_{z>z_i}p_z(\sigma_j)\sum_{z>z_j}p_z(\sigma_j)\\&\quad+\phi(\sigma_j)^2\sum_{z>\max(z_i,z_j)}\Delta^2(p_z(\sigma_j)),\end{aligned}\tag{A6}$$

where with Δ^2 we indicate the associated variances. We neglected the cross-correlation terms in Equation (A6) as we consider the uncertainties in p_z and $\Phi(\sigma)$ to be independent. We also assume the uncertainties $\Delta p_z(\sigma_j)$ relative to different bins of age to be independent. The uncertainties $\Delta p_z(\sigma_j)$ include Poisson errors, random errors (see Haiman et al. 2007), plus a systematic $\Delta p_z(\sigma_j) = 0.5 \times p_z(\sigma_j)$ uncertainty associated with the method to compute ages which redistributes galaxies in a given bin (see Figure 1 in Haiman et al. 2007). When computing the variances associated with the highest redshift bins, we sum up 50% of the uncertainties of all the lowest redshift bins, i.e., $0.5 \times \sum_z \Delta p_z(\sigma_j)$, given that the uncertainty in the highest-z bins depends on the overall uncertainties in the lowest redshift bins. Finally, we also add in quadrature in the covariance matrix the systematic uncertainties of ± 1 Gyr in the ages, which translate into an uncertainty in the accreted mass at each epoch (gray area in Figure 2).

The covariance matrix expressed in Equation (A4) can be greatly simplified by noting that when convolving the VDF with a Gaussian with dispersion η, the resulting BH mass density is correlated with the scatter-free BH mass density as (see Marconi et al. 2004 for details)

$$\rho_{\mathrm{VDF},\eta} = \exp\left[0.5\,(\eta\ \ln 10)^2\right] \times \rho_{\mathrm{VDF},0}\,. \tag{A7}$$

Note, also, that the scatter-free BH mass function is simply equal to the VDF times the Jacobian factor J, i.e., $\phi[M_{\mathrm{BH,k}}(\sigma_j, z_i)] = \phi(\sigma_j) \times J$, with $J = |d\log\sigma/d\log M_{\rm BH}| = 3.83$ (see Equation (2)) and $M_{\mathrm{BH,k}}(\sigma_j, z_i)$ given by Equation (2) at z_i and σ_j. Equation (A3) will then simply read as

$$\begin{aligned}C_{ij} &= \left\{\exp\left[0.5\,(\eta\ \ln 10)^2\right]\right\}^2 \mathrm{COV}(\Delta\rho_{\mathrm{VDF},0}(z_i), \Delta\rho_{\mathrm{VDF},0}(z_j))\\&= \left\{\exp\left[0.5\,(\eta\ \ln 10)^2\right]\right\}^2 \sum_k M_{\mathrm{BH,k}}^2\\&\quad\times\left\{\left[\sum_j \mathrm{COV}\left(\Delta\left(\phi\left[M_{\mathrm{BH,k}}(\sigma_j, z_i)\right]\sum_{z>z_i}p_z(\sigma_j)\right),\right.\right.\right.\\&\quad\left.\left.\left.\Delta\left(\phi\left[M_{\mathrm{BH,k}}(\sigma_j, z_j)\right]\sum_{z>z_j}p_z(\sigma_j)\right)\right)\right]\right\}.\end{aligned}\tag{A8}$$

The errors computed on $\rho_\bullet(z)$ following the method described above are only a *lower* limit to the true uncertainties. The total error budget, in fact, includes several other uncertainties not taken explicitly into account in the above formalism, such as, e.g., systematics in the adopted scaling relations, in the assumed intrinsic scatter, hidden correlations. We therefore choose to increase the overall errors $\Delta\rho_\bullet(z)$ by a factor of 2, thus rendering the uncertainties in $\rho_\bullet(z)$ of the order of $\sim 20\%$–30%, comparable to what estimated in a full Monte Carlo approach (see Marconi et al. 2004; Shankar & Ferrarese 2009).

In the paper we then adopt Equations (A8) and (A6) for estimating the covariance matrix associated with a given model and then compute χ^2 as

$$\chi^2 = \sum_i \sum_j \left[\rho_\bullet(z_i) - \rho_{\mathrm{VDF}}(z_i)\right] C_{ij} \left[\rho_\bullet(z_j) - \rho_{\mathrm{VDF}}(z_j)\right]. \tag{A9}$$

When computing the covariance matrix we do not include the first bin of $\rho_\bullet(z)$ at $z = 0$ because it is equal (i.e., maximal correlation) to the BH mass density at $\rho_\bullet(z)$ at $z = 0.2$, given that the fraction of early-type galaxies formed below $z = 0.2$ is negligible.

REFERENCES

Bell, E. F., Zheng, X. Z., Papovich, C., Borch, A., Wolf, C., & Meisenheimer, K. 2007, ApJ, 663, 834
Bernardi, M., Nichol, R. C., Sheth, R. K., Miller, C. J., & Brinkman, J. 2006, AJ, 131, 1288
Bernardi, M., Sheth, R. K., Tundo, E., & Hyde, J. B. 2007, ApJ, 660, 267
Cattaneo, A., & Bernardi, M. 2003, MNRAS, 344, 45
Cavaliere, A., Giallongo, E., Vagnetti, F., & Messina, A. 1982, A&A, 114, 1
Ciotti, L., Lanzoni, B., & Volonteri, M. 2007, ApJ, 658, 65
Cirasuolo, M., Shankar, F., Granato, G. L., De Zotti, G., & Danese, L. 2005, ApJ, 629, 816
Coppin, K., et al. 2009, MNRAS, 389, 45
De Zotti, G., Shankar, F., Lapi, A., Granato, G. L., Silva, L., Cirasuolo, M., Salucci, P., & Danese, L. 2006, MmSAIt, 77, 661
Drory, N., & Alvarez, M. 2008, ApJ, 680, 41
Drory, N., Salvato, M., Gabasch, A., Bender, R., Hopp, U., Feulner, G., & Pannella, M. 2005, ApJ, 619, 131
Dunkley, J., et al. 2009, ApJS, 180, 306
Eddington, A. S. 1922, MNRAS, 83, 32
Faber, S. M., et al. 2007, ApJ, 665, 265
Ferrarese, L. 2002, ApJ, 578, 90
Ferrarese, L., & Merritt, D. 2000, ApJ, 539, L9
Fontanot, F., Cristiani, S., Monaco, P., Nonino, M., Vanzella, E., Brandt, W. N., Grazian, A., & Mao, J. 2007, A&A, 461, 39
Gebhardt, K., et al. 2000, ApJL, 539, 13
Gould, A. 2003, arXiv:astro-ph/0310577
Graham, A. W. 2007, MNRAS, 379, 711
Haiman, Z., Ciotti, L., & Ostriker, J. P. 2004, ApJ, 606, 763
Haiman, Z., Jimenez, R., & Bernardi, M. 2007, ApJ, 658, 721
Haring, N., & Rix, H. W. 2004, ApJ, 604, L89
Heavens, A. F., Jimenez, R., & Lahav, O. 2000, MNRAS, 317, 965
Ho, L. C., Darling, J., & Greene, J. E. 2007, ApJ, 669, 821
Hopkins, P. F., Richards, G. T., & Hernquist, L. 2007, ApJ, 654, 731
Hopkins, P. F., Robertson, B., Krause, E., Hernquist, L., & Cox, T. J. 2006, ApJ, 652, 107
Jimenez, R., Bernardi, M., Haiman, Z., Panter, B., & Heavens, A. F. 2007, ApJ, 669, 947
Kollmeier, J. A., et al. 2006, ApJ, 648, 128
Lauer, T. R., Tremaine, S., Richstone, D., & Faber, S. M. 2007, ApJ, 670, 249
Loeb, A., & Peebles, P. J. E. 2003, ApJ, 589, 29
Lotz, J. M., et al. 2008, ApJ, 672, 177
Magorrian, J., et al. 1998, AJ, 115, 2285
Marconi, A., & Hunt, L. K. 2003, ApJ, 589, L21
Marconi, A., Risaliti, G., Gilli, R., Hunt, L. K., Maiolino, R., & Salvati, M. 2004, MNRAS, 351, 169
McLure, R. J., & Dunlop, J. S. 2004, MNRAS, 352, 1390
McLure, R. J., Jarvis, M. J., Targett, T. A., Dunlop, J. S., & Best, P. N. 2006, MNRAS, 368, 1359
Merloni, A., et al. 2004, MNRAS, 353, 1035
Merloni, A., & Heinz, S. 2008, MNRAS, 388, 1011
Merloni, A., Rudnick, G., & Di Matteo, T. 2005, MNRAS, 354, 37
Netzer, H., & Trakhtenbrot, B. 2007, ApJ, 654, 754
Peng, C. Y. 2007, ApJ, 671, 1098
Peng, C. Y., Impey, C. D., Rix, H. W., Kochanek, C. S., Keeton, C. R., Falco, E. E., Lehár, J., & McLeod, B. A. 2006, ApJ, 649, 616
Pérez-González, P. G., et al. 2008, ApJ, 675, 234
Richards, G. T., et al. 2006, ApJS, 166, 470
Salpeter, E. E. 1964, ApJ, 140, 796
Salucci, P., et al. 1999, MNRAS, 307, 637
Shankar, F., Crocce, M., Miralda Escudé, J., Fosalba, P., & Weinberg, D. H. 2008, ApJ, submitted (arXiv:0810.4919)

Shankar, F., & Ferrarese, L. 2009, ApJ, submitted
Shankar, F., & Mathur, S. 2007, ApJ, 660, 1051
Shankar, F., Salucci, P., Granato, G. L., De Zotti, G., & Danese, L. 2004, MNRAS, 354, 1020
Shankar, F., Weinberg, D. H., & Miralda Escudé, J. 2009, ApJ, 690, 20 (SWM)
Shen, J., Vanden Berk, D. E., Schneider, D. P., & Hall, P. B. 2008a, AJ, 135, 928
Shen, Y., et al. 2007, AJ, 133, 2222
Shen, Y., et al. 2008b, ApJ, 680, 169
Sheth, R. K., et al. 2003, ApJ, 594, 225
Shields, G. A., Menezes, K. L., Massart, C. A., & Vanden Bout, P. 2006, ApJ, 641, 683
Silk, J., & Rees, M. J. 1998, A&A, 331, L1
Silverman, J. D., et al. 2008, ApJ, 679, 118
Small, T. A., & Blandford, R. D. 1992, MNRAS, 259, 725
Sołtan, A. 1982, MNRAS, 200, 115
Spergel, D. N., et al. 2007, ApJS, 170, 377
Thomas, D., Maraston, C., Bender, R., & Mendes de Oliveira, C. 2005, ApJ, 621, 673
Trager, S. C., Faber, S. M., Worthey, Guy, & González, J. Jesús 2000, AJ, 119, 1645
Treu, T., et al. 2007, ApJ, 667, 117
Tundo, E., Bernardi, M., Hyde, J. B., Sheth, R. K., & Pizzella, A. 2007, ApJ, 663, 53
Vestergaard, M. 2004, ApJ, 601, 676
Woo, J. H., Treu, T., Malkan, M. A., & Blandford, R. D. 2008, ApJ, 681, 925
Wyithe, J. S. B. 2004, MNRAS, 1082, 1098
York, D. G., et al. 2000, AJ, 120, 1579
Yu, Q., & Tremaine, S. 2002, MNRAS, 335, 965
Zhao, D. H., et al. 2003, MNRAS, 339, 12